Journal of Structural Geology, Vol. 7, No. 6, pp. 651 to 666, 1985
Printed in Great Britain

0191-8141/85 $03.00 + 0.00

Patterns of deformed early lineations over later folds formed by buckling and flattening

S. K. GHOSH and A. CHATTERJEE

Department of Geological Sciences, Jadavpur University, Calcutta 700 032, India

(*Received* 1 *August* 1984; *accepted in revised form* 3 *December* 1984)

Abstract—The patterns of deformed early lineations (L_1) over later folds (F_2) can be classified into several morphological types depending on the nature of variation of $L_1 \wedge F_2$ over the folds. The field relations indicate that the folds under consideration are neither shear folds nor parallel folds modified by flattening. The lineation patterns are therefore interpreted in terms of an empirical model of simultaneous buckling and flattening in which it is assumed that (i) the central surface of the folded layer remains a sine curve in transverse profile, (ii) the ratio of rates of buckle shortening to homogeneous strain is proportional to $\sin 2\alpha$, with α as the dip angle and (iii) the progressive deformation is coaxial with the Z-axis of bulk strain parallel to the planar segments of the early folds. The model gives an insight into the relative importance of different physical factors which control the development of dissimilar lineation patterns. Not all lineation patterns are explicable by this simplified model. Thus complex patterns with variable $L_1 \wedge F_2$ along the fold axis may develop by a progressive rotation of the geometrically defined fold hinge through successive material lines. The theoretical results have been applied to interpret the lineation patterns in Central Rajasthan, India. It is concluded that L_1 was initially very close to the E–ESE trending subhorizontal Z-axis of bulk deformation during F_2-folding and that the X-axis was subhorizontal or gently plunging with a N–NNE trend.

INTRODUCTION

EARLY lineations (say L_1) which can be straightened out by unrolling the later folds (say F_2) are common in areas of superposed deformations. Such unrollable early lineations indicate that the later folds had developed by flexural slip. Moreover, when the later folds are diversely oriented, the initial orientation of L_1 can be determined from the intersection of lineation loci (Ramsay 1967, p. 549). Lineations which remain curvilinear when the fold is unrolled are much more difficult to utilize in a structural analysis, since the development of a specific type of the lineation pattern is controlled by a large number of factors. Ramsay (1960, 1967) has considered several circumstances in which the angle between L_1 and the F_2 axis could vary over the same fold and this analysis was further extended by Hudleston (1973a, pp. 126–130).

A systematic morphological classification of deformed lineation patterns was made by Mukhopadhyay & Ghosh (1980) who recognized three principal types of deformed L_1 lineation. The classification was based on whether the acute angle between L_1 and the F_2 axis does or does not open in the same sense on the two limbs of F_2, whether $L_1 \wedge F_2$ is constant or variable and whether the lineation does or does not lie on a plane. The notation '$L_1 \wedge F_2$' will be used throughout to refer to the angle between L_1 and the axis of F_2.

Representation of deformed L_1 and recognition of dissimilar lineation patterns are most conveniently done when, along with the plots of L_1 and F_2 axes in equal-area projection, the pattern of deformed L_1 is represented in a plane obtained by unrolling the form surface of F_2. The latter pattern can be directly obtained by placing a transparent overlay on the mesoscopic folds and drawing the lineation on it. The lineation patterns of several folds drawn on such transparent overlays have been described by Naha & Halyburton (1977a).

The pattern of a deformed L_1 over F_2 is controlled essentially by (1) the competence contrast of the associated rocks, (2) the initial orientation of the planar segment of F_1 on which L_1 lies, (3) the initial angle between L_1 and F_2 and (4) the nature and intensity of bulk deformation. The planar segment may either be the F_1 axial plane cleavage or a small segment of the form surface of a tight F_1 fold. In the following analysis we make an attempt to find out whether the lineation patterns can give us significant information about the controlling physical factors.

The present investigation started with an analysis of patterns of deformed early lineations over a large number of mesoscopic folds in Central Rajasthan and in certain selected localities of Bihar and Karnataka, India. We found that the morphological classification of Mukhopadhyay & Ghosh (1980) can be considerably enlarged. In the following analysis we present in turn (i) the structural background of superposed deformation in Central Rajasthan, (ii) a general morphological classification of lineation patterns, (iii) a theoretical model of folding of L_1 by simultaneous external rotation and flattening, (iv) an analysis of the lineation patterns obtained by numerical calculations from the theoretical model, (v) an interpretation of complex patterns, including curved lineations on a planar surface and (vi) an application of the theoretical results to interpret the lineation patterns in Central Rajasthan. The major part of the mathematical development of the model is given in the Appendix.

SUPERPOSED DEFORMATIONS IN CENTRAL RAJASTHAN

The Precambrian gneisses and schists belonging to the Banded Gneissic Complex and the Aravalli Supergroup of Central Rajasthan, India, show a well-developed lineation parallel to the axis of early isoclinal folds (F_1). The lineation which appears either as a mineral lineation or as a striping in migmatites, mica schists, quartzites, amphibolites, marbles and calc-schists, has been deformed during the development of later upright folds (F_2). The complex shapes of the folds resulting from superposition of F_1 and F_2 have been subjected to detailed analysis by Naha and others (Naha & Halyburton 1977a,b, Naha 1983, Roy & Jain 1974, Roy *et al.* 1981). These analyses show that although in detail their axial surfaces and hinges show large variations in attitude, the early folds have an overall E–ESE trend and are reclined in most places. In contrast the F_2 axial surfaces show a small range of variation in attitude; they are usually subvertical with a N–NNE strike. As a result, the F_2 fold hinges show a more or less uniform trend but a large range in plunge. It may be noted that the folds under consideration do not occur in shear zones; moreover, as shown below, they are not passive folds. Hence, the consistently upright character of the folds over a very large area and the constancy in orientation of their axial planes, irrespective of the variation in tightness of the F_2 folds, would indicate that the bulk deformation during the development of F_2 was by and large coaxial with the Z-axis subhorizontal and trending E–ESE.

The mesoscopic F_2 folds are often disharmonic and with larger folds developing on thicker units. The plots of t'_α (Ramsay 1967) against α and of ϕ_α (Hudleston 1973b) against α of a large number of folds by Naha & Halyburton (1977a & b) show that the majority of folds belong to $1B$, $1C$ or Class 3 of Ramsay. Our observations show that the most common mesoscopic folds in all the stratigraphic units show a combination of Class $1C$ and Class 3 types in alternating competent and incompetent units. Again, the early lineation in competent units often shows a small circle pattern of distribution (Naha & Halyburton 1977a, p. 101, Mukhopadhyay & Ghosh 1980). All these features indicate that F_2 had developed by buckling. From the Fatehpur area of Rajasthan, Mukhopadhyay & Ghosh (1980) have given additional evidence for rejecting the shear folding mechanism for the development of F_2. They have shown that the geometrical configuration of the assumed 'a' directions gives results quite incompatible with the model of shear folding. Evidently the patterns of non-unrollable early lineations have to be explained by some mechanism other than shear folding.

PATTERNS OF DEFORMED LINEATIONS

The patterns of deformed L_1 over F_2 can be classified into the following types, illustrated on the unrolled form surface of F_2 in Fig. 1. Excepting type 6, the ends of the lineation loci in Fig. 1 lie on the inflection lines of the folds.

Type 1. $L_1 \wedge F_2$ is constant. The lineation can be unrolled.

Type 2. $L_1 \wedge F_2$ is a minimum at the hinge and increases away from it on both limbs. The sense of curvature of L_1 is opposite on the two limbs.
(a) $L_1 \wedge F_2$ does not become 90° anywhere. On the unrolled form surfaces the pattern of L_1 shows a twofold rotation symmetry.
(b) $L_1 \wedge F_2$ does not become 90° anywhere and the lineation pattern does not show a rotation symmetry.
(c) $L_1 \wedge F_2$ changes through 90° on one limb only.

Type 3. $L_1 \wedge F_2$ increases from one line of inflection of the fold to the other and maintains the same sense of curvature everywhere.
(a) $L_1 \wedge F_2$ does not exceed 90° anywhere.
(b) $L_1 \wedge F_2$ exceeds 90° on one limb.

Type 4. $L_1 \wedge F_2$ is 90° at the hinge only and shows a mirror symmetry about the hinge line on the unrolled form surface. The sense of curvature is the same everywhere.

Type 5. $L_1 \wedge F_2$ is a maximum at the hinge and decreases on either side. The sense of curvature is opposite on the two limbs.
(a) On the unrolled form surface there is a two-fold rotation symmetry.
(b) On the unrolled form surface there is no rotation symmetry.

Type 6. Complex patterns characterized by variable $L_1 \wedge F_2$ along the fold axis.

For a rigorous classification the lineation on the unrolled form surface may be depicted as a curve $y = f(x)$, with y parallel to the hinge line and x perpendicular to it (Fig. 1). The dissimilar patterns can then be classified on the basis of variation of $|dy/dx|$, dy/dx, d^2y/dx^2, presence or absence of mirror symmetry or rotation symmetry and the occurrence of a stationary point.

Among all these categories only the type 1 pattern shows a small circle locus on a stereoplot; it gives a great circle distribution only when $L_1 \wedge F_2 = 90°$. The majority of the other types fall neither on small circles nor on great circles. Although we have noted in each case whether a folded lineation lies on a plane or not, the following arguments show that this information need not be a basis for a classification of deformed lineation patterns. Although in many cases the patterns show an approximate great circle distribution, there are small but consistent deviations near the hinge zones of the folds. Only in a few cases did we find a consistent great circle distribution. Moreover, approximate great circle distribution patterns are often closely associated with other patterns in neighbouring outcrops. Hence the great

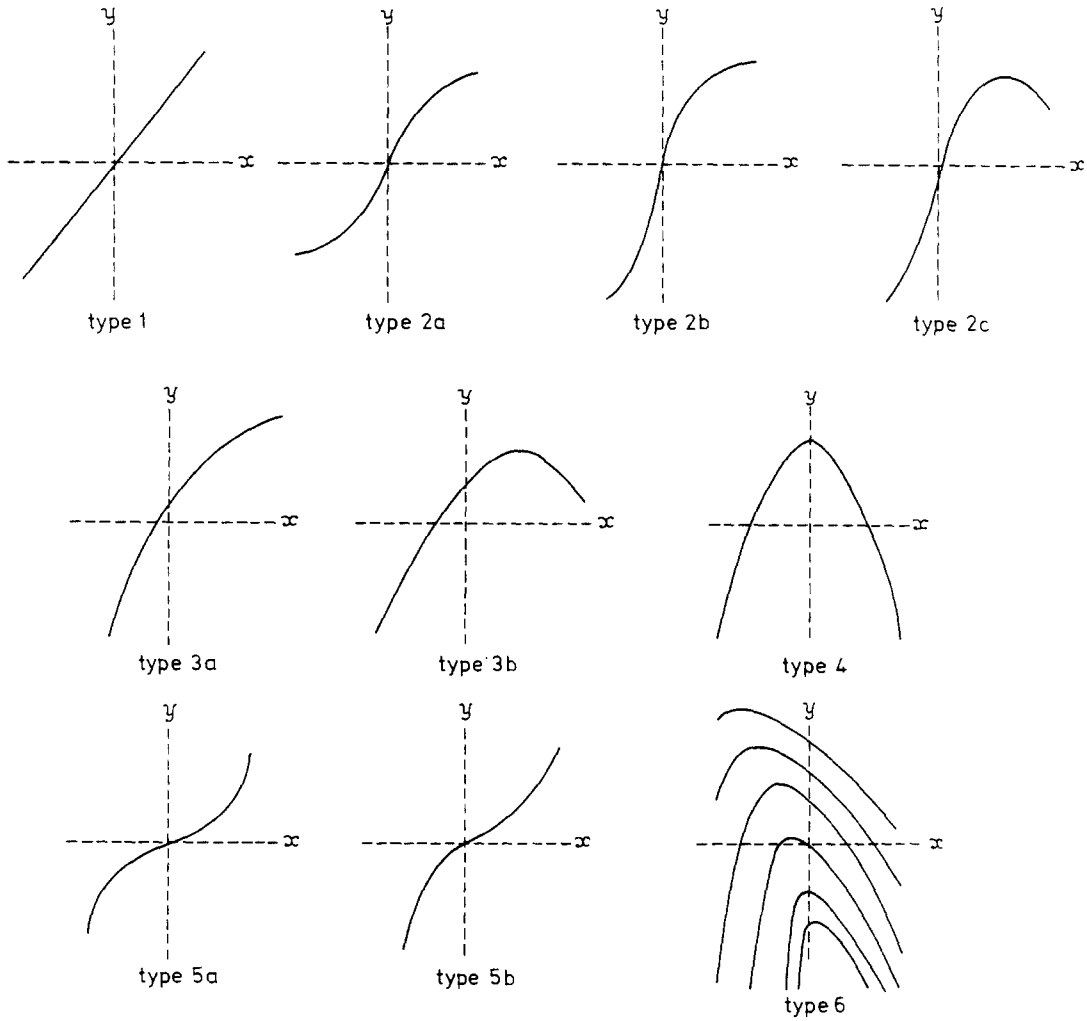

Fig. 1. Classification of lineation patterns on the unrolled form surface. The hinge line of F_2 is along the y axis.

circle pattern is not diagnostic for a particular fold mechanism.

Among the mesoscopic folds of Rajasthan, the type 1 pattern is common in the competent units. In the less competent rocks, type 2(b) is often seen. Types 3 and 4 are fairly common in many localities. Both types 5 and 6 are rare. Some of the lineation patterns are shown in Figs. 2 and 3.

The ten-fold classification of lineation patterns presented here (Fig. 1) originated from our field observations, in Rajasthan and elsewhere, as well as from numerical calculations of the theoretical model described later. While striking differences among some of the natural examples were immediately apparent, it was the numerical modelling which emphasized the importance of classifying the lineation patterns on the basis of symmetry, the presence of a stationary point or the presence of an inflection point (Fig. 1). Thus the numerical models showed us that symmetrical forms of type 2(a) or type 4 developed only under very special situations. The model also emphasized the connectedness of some of the patterns, such as the transformation of 2(b) into 2(c) or 3(a) into 3(b) with progressive deformation.

THEORETICAL MODEL

General

We have already shown that the mesoscopic folds observed by us are not shear folds and hence the lineations are not deformed by unequal slip along planes parallel to the axial plane. Moreover, it will be shown later that the type 4 pattern could have been produced only where L_1 was initially at 90° to the F_2 axis. Since even in this case the final pattern of lineation does not necessarily lie on a plane, we conclude that the folds are not parallel folds modified by flattening. It is therefore justified to start with the working hypothesis that the deformation of L_1 was achieved by the combined effects of simultaneous external rotation and homogeneous strain. The importance of such a mechanism has been emphasized by several authors (Ramsay 1967, Hudleston 1973b, Hobbs *et al.* 1976) and is inherent in the models of buckle folding of Biot (1965) and Ramberg (1964).

No doubt the following analysis would have been very much simpler if we had chosen Hudleston's (1973b) model of simultaneous buckling and flattening. How-

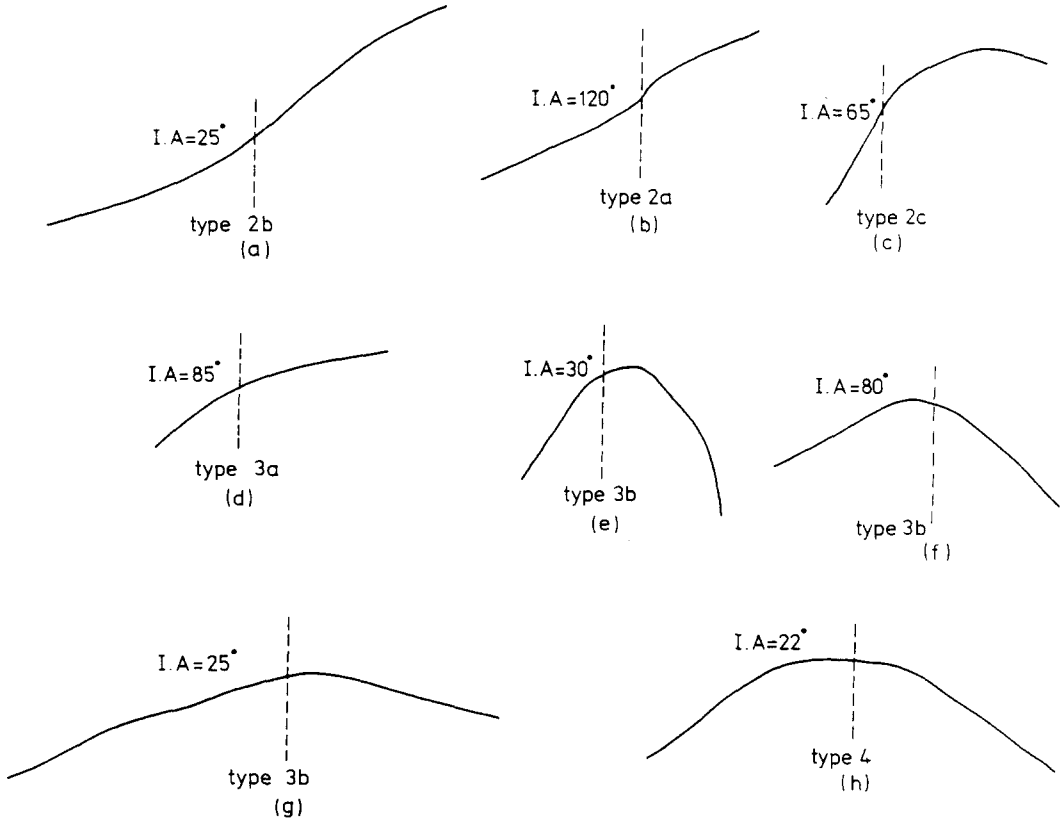

Fig. 2. Natural patterns of deformed L_1 after unrolling F_2. Dashed line, F_2 hinge; I.A. interlimb angle. Mesoscopic folds from Central Rajasthan.

ever, although Hudleston's model has proved useful in the interpretation of plots of t'_α against α for natural and experimental folds, it is not so suitable for our purpose of interpreting deformed lineation patterns, since the model is concerned with a special situation in which the orientation of the fold axis or the profile plane remains constant during progressive deformation. Moreover, in this model the rotation increments at a point of inflection remain constant at all stages of folding, and since the flattening increments are also constant, the ratio between the rates of rotation and flattening remains unchanged in progressive folding. Although the shape of the folded surface is not specified in Hudleston's model, his equations do impose certain constraints on the fold shape. Thus, if ds is taken as the arc-length of a small segment of the folded surface, his eqn. (4) implies that the curvature dα/ds remains constant all over the fold. In the extreme case of parallel folding, when the flattening increment is negligibly small in comparison with the rotation increments his eqn. (19) also implies that dα/ds remains constant and the folded surface remains a circular arc at all stages of folding.

Our model is also idealized as all such models have to be; the necessity for simplification arises from our incomplete knowledge about the mechanics of buckle folding at large amplitudes. Our model contains three assumptions. (1) The central surface of the folded layer in transverse profile remains a sine curve at all stages of folding. (2) The ratio of the rates of buckle shortening ($\dot{\varepsilon}'_3$) and of layer-parallel homogeneous strain ($\dot{\varepsilon}_3$) is given by the empirical relation

$$\frac{\dot{\varepsilon}'_3}{\dot{\varepsilon}_3} = A \sin 2\alpha, \tag{1a}$$

with

$$\varepsilon'_3 = \frac{\Delta b}{b}, \tag{1b}$$

where α is the dip angle (with reference to the hinge) of the fold at the point of inflection, b is the quarter wavelength and A is a constant dependent on the competence contrast of the associated rocks. (3) The progressive deformation is coaxial with the Z-axis of bulk strain during F_2-folding parallel to the planar segment of an early fold.

The buckling equations of Ramberg (1964) show that the ratio of buckle-shortening to layer-parallel homogeneous strain is proportional to the square of the amplitude–wavelength ratio. However, as stated by Ramberg, this relation is valid only for gentle sinusoidal folds. It is well-known that at large values of amplitude–wavelength ratios, the limbs tend to approach a 'locked position' and the ratio of the rates of buckle shortening to homogeneous strain is greatly reduced. Clearly we need an expression for this ratio which is zero when the layer is straight, reaches a maximum at some intermediate stage of folding and again vanishes when the fold tends to become isoclinal. These conditions are satisfied by our assumption that for small increments of bulk deformation, the ratio of the rates of buckle-shortening to homogeneous strain is proportional to sin 2α. For steady deformation, we have from eqn. (1a)

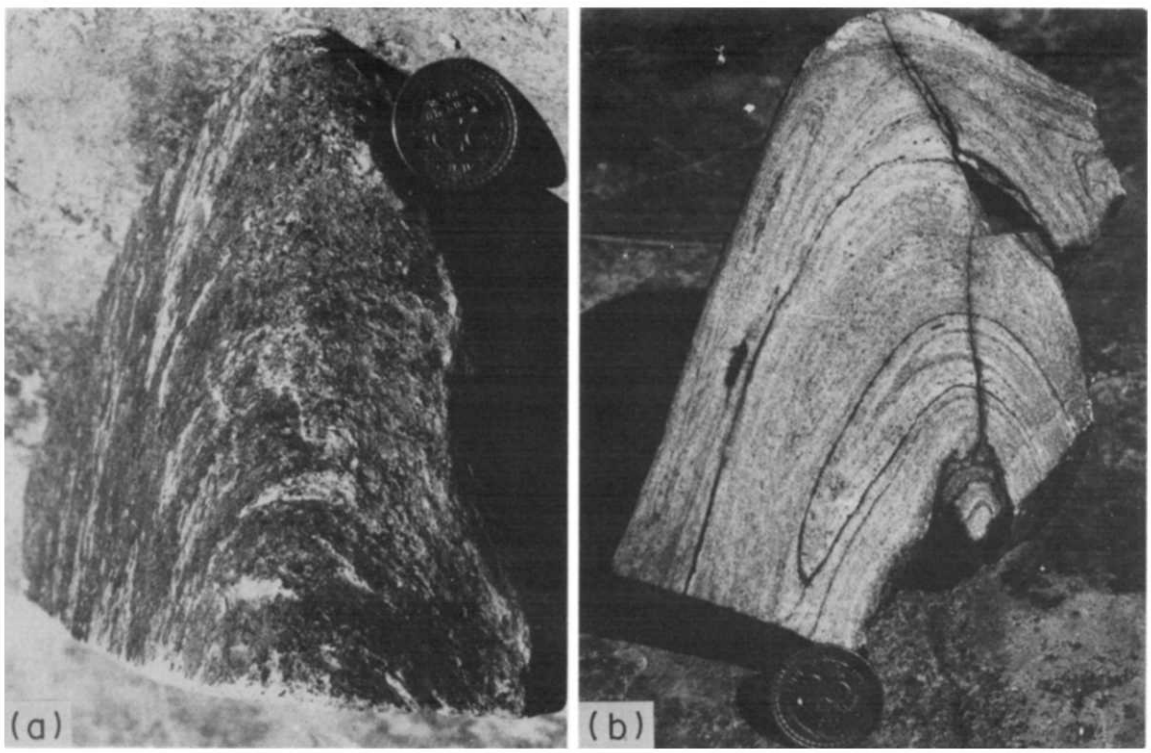

Fig. 3. (a) Type 4 pattern of deformed L_1 over F_2 hinge from Bhindar region, Rajasthan. (b) Profile section of same specimen showing folded axial surface of early isoclinal fold. The coin is nearly 2 cm in diameter.

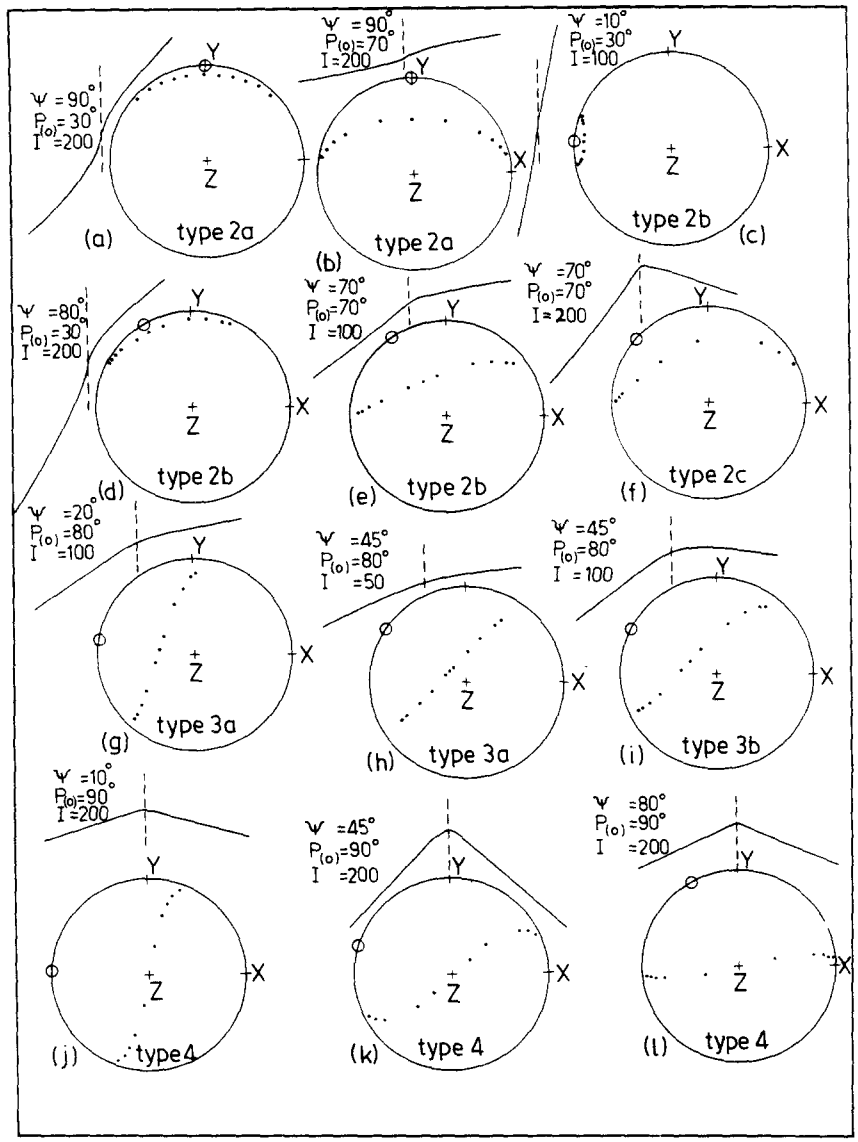

Fig. 4. Patterns of deformed lineations obtained from the theoretical model for $\lambda_1 \neq \lambda_2$. Patterns are shown both in equal-area projection (open circle, F_2 axis; dots, L_1) and on the unrolled form surface. The dashed lines are F_2 hinges. The fold is unrolled to a plane containing F_2 and Z axes. I = number of cycles of incremental strain. In (c), the value of A is 5; otherwise $A = 2$. Note that the 2(b) pattern in (e) changes to a 2(c) pattern in (f) and that the 3(a) pattern in (h) changes to a 3(b) pattern in (i) with progressive deformation. Among type 4 patterns, $\psi = 45°$ gives the maximum curving of L_1 for the same deformation. The very small variation in $L_1 \wedge F_2$ in (c) is due to the small value of ψ.

$$\Delta\varepsilon_3' = A \sin 2\alpha . \Delta\varepsilon_3. \quad (2)$$

Thus we assume that in successive small intervals of time, the incremental shortenings along the Z-axis are successively $\Delta\varepsilon_3$ and $\Delta\varepsilon_3'$. If we keep $\Delta\varepsilon_3$ constant, as we have done in the numerical calculations, the buckle shortening increases from zero when the layer is straight to a maximum value of $A\Delta\varepsilon_3$ at an interlimb angle of 90° and then decreases with progressive tightening of the fold. The advantage of choosing a sine curve for the fold profile is that it remains a sine curve after an incremental homogeneous strain.

Our third assumption is not independent; it is indeed a corollary of the first assumption. The assumption of sinusoidal folding means that we consider only symmetrical folds and hence the necessity of assuming a progressive coaxial deformation with the bedding parallel to the direction of maximum compression. It is merely a fortunate coincidence that in Central Rajasthan, the major area of our study, the bulk deformation during F_2-folding can be interpreted to have been more or less coaxial.

The present model of simultaneous homogeneous strain and external rotation was approximated by repeated alternations of small increments of strain and rotation. We have chosen the coordinate axes x_1, x_2 and x_3 along X, Y and Z axes of bulk strain. We start with a planar structure (S) parallel to x_3. Its trace (F) on the x_1x_2-plane makes an initial angle ψ with the x_1 axis. A lineation (L) makes an angle (P) with F. The successive stages of deformation considered in the model are summarized below. (1) Initial stage: during this stage the initial plane and lineation undergo a change in orientation by an initial homogeneous strain (step 1). This is followed by a stage of initial buckling (step 2) through a small angle. In the numerical calculations this rotation

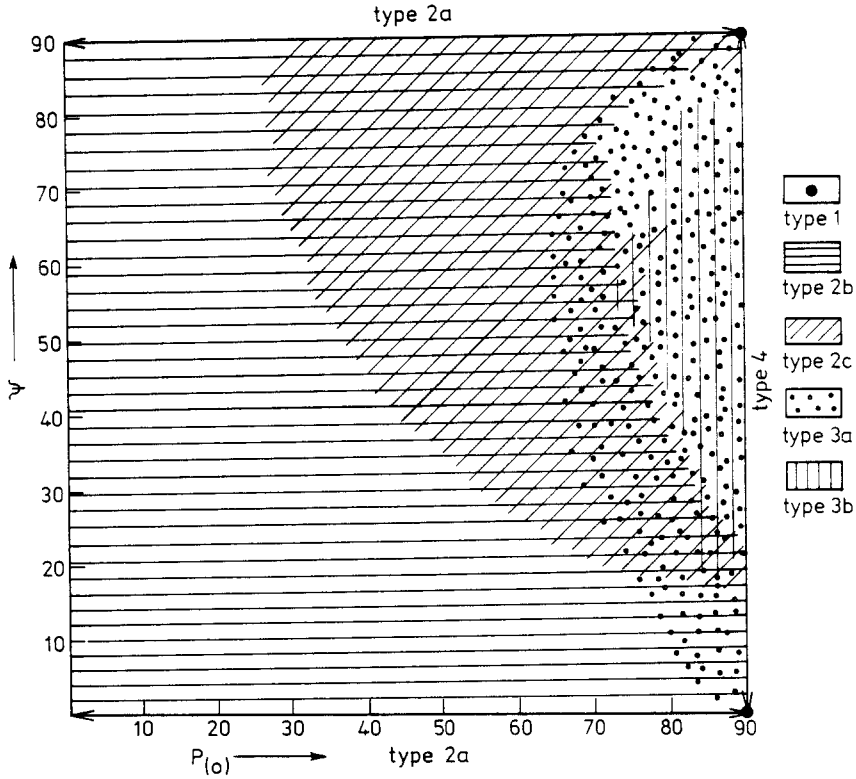

Fig. 5. The fields of dissimilar lineation patterns in a ψ-$P_{(0)}$ diagram as obtained from numerical calculations for $\lambda_1 \neq \lambda_2$. The 2(a) patterns occur along lines $\psi = 0°$ and $\psi = 90°$. Type 4 patterns occur along a line $P_{(0)} = 90°$. The overlapping of fields is generally produced by the change from one pattern to another with progressive deformation.

was 1° for each limb. Thus, we start with an initial folded surface which in the profile plane is a sine curve dipping 1° on either side at the points of inflection. (2) Main stage: this consists of repeated alternations of incremental homogeneous strain (step 3) and incremental buckling (step 4). A sine curve in the profile plane remains a sine curve during the homogeneous strain. The length of arc of the sine curve changes during an increment of homogeneous strain but remains unaltered during an increment of buckle shortening. We have presented the mathematical development of the model through eqns. (3)–(35) in the Appendix and the orientation of F and those of S and L at different points of the fold are traced through the successive increments of flattening and buckling.

In natural folds in layers with sufficient competence contrasts, the buckling and flattening are strictly simultaneous, and the instantaneous strain is inhomogeneous over a folded surface. On the other hand, the alternation of small increments of buckling and homogeneous flattening in our model is an artifice to approximate simultaneous buckling and flattening; hence instantaneous strain distribution over the fold is not relevant for our model. Rather, we have to consider the strain distribution over a small interval consisting of a few cycles of steps 3 and 4 of our model, provided each of these steps is sufficiently small. Over such a small interval the strain in our model will be inhomogeneous along a folded surface. Moreover, over such intervals, the local deformations in the fold-limbs will be non-coaxial. Nevertheless, the inhomogeneous strain distribution in natural folds is likely to be more complex than in our idealized model. While applying the theoretical results to actual field examples we should therefore avoid interpretations based on small differences in lineation patterns.

Numerical calculations

The numerical calculations were done using a computer, after the first two steps, by repeating 200 times each cycle consisting of steps 3 and 4, the output data of each cycle being taken as the initial data of the next cycle. The computations were done with three values of A, namely 0.5, 2 and 5. It may be recalled that increasing values of A means increasing competence contrasts. The three values chosen here represent moderately low, fairly high and very high competence contrasts. For each A, the angle (ψ) between the x_1 axis and the trace of $S_{(0)}$ on the x_1x_2-plane was chosen as 0, 5, 10, 20, 45, 70, 80, 85 and 90°. Again, for each of these cases the initial angle $P_{(0)}$ between the lineation and the trace of S on the x_1x_2 plane was chosen as 10, 30, 50, 60, 70, 80, 85 and 90°. Lastly for each case three types of incremental homogeneous deformation were chosen: (1) $\Delta\varepsilon_2 = 0$, (2) $\Delta\varepsilon_1 = \Delta\varepsilon_2$ and (3) $\Delta\varepsilon_1 = 2\Delta\varepsilon_2$. These three cases represent respectively the plane-strain type, the uniaxial oblate type and a flattening type of strain ellipsoid (Ramsay 1967). For all these cases the initial homogeneous strain along the x_3-axis was -0.1, the initial external rotation was 1° on either side at each point of inflection and the incremental homogeneous strain $\Delta\varepsilon_3$ for each cycle was

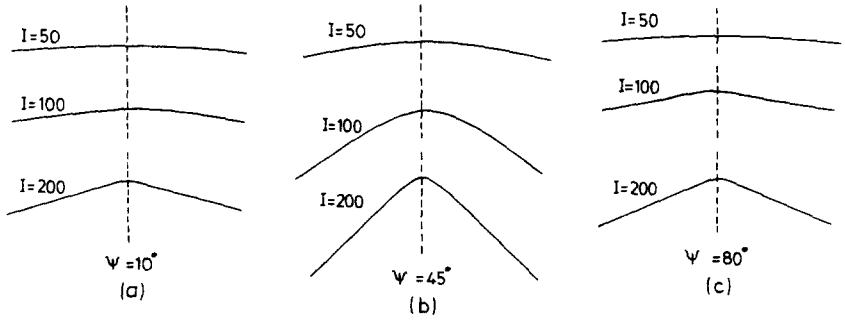

Fig. 6. Three stages of development of type 4 patterns on unrolled form surfaces for (a) low, (b) intermediate and (c) high values of ψ. I, number of cycles of incremental deformation; dashed lines, F_2 hinges. Note that a strong curvature of L_1 is comparatively easily obtained when ψ has intermediate values. At low or high values of ψ, $L_1 \wedge F_2$ changes very slowly at the limbs. $A = 2$ in all cases.

-0.005. The deformation was considered to be isochoric. In each case the direction cosines of S and L were computed at 11 points of the fold profile, including the hinge point, two inflection points and four intermediate points on either flank. To study the progressive change in lineation pattern, the output data for each case were obtained at 10, 50, 100 and 200 cycles of incremental deformations.

The data were plotted in equal-area projections with the x_3-axis vertical so that the fold axis would plot at the periphery and deviations from small and great circle patterns would be easy to recognize. In addition the deformed patterns of lineation on the unrolled form surface were reconstructed from the values of P at the eleven points on the fold profile (Fig. 4). The arc-length distances of each of these points were calculated from eqn. (33a).

A convenient way of synthesizing this large volume of data is to plot the dissimilar lineation patterns with different symbols on a ψ-$P_{(0)}$ diagram (Fig. 5) in order to delineate approximately the separate or overlapping fields. It should be noted that Fig. 5 represents the cases in which $\lambda_1 \neq \lambda_2$. When $\lambda_1 = \lambda_2$ we get only two types of lineation pattern, that is type 1 when $P_{(0)} = 90°$ and type 2(a) when $0 < P_{(0)} < 90°$.

DEVELOPMENT OF DISSIMILAR LINEATION PATTERNS

The present study is essentially concerned with lineations which cannot be unrolled; hence, we avoided very large values of A in the numerical calculations. As test cases we made only a few computations with $A = 20$. At such very large values of A the ratio of the rates of buckle-shortening to homogeneous strain remained very large till quite a mature stage of folding and the lineation pattern showed a small or negligible deviation from the type 1 pattern. A significant variation in $L_1 \wedge F_2$ over the fold could be seen when the total shortening was very large. For moderate competence contrasts and $\lambda_1 \neq \lambda_2$, a type 1 pattern may develop when $P_{(0)}$ or the initial angle between L_1 and the F_2 axis is equal to 90° while the F_2 axis is parallel to either X or Y. When $\lambda_1 = \lambda_2$ and $P_{(0)} = 90°$, the type 1 pattern will form at all values of ψ.

The maximum information about the controlling factors is obtained from the type 4 lineation pattern. Presumably its mirror symmetry can only develop under a restricted set of conditions: (i) with essentially coaxial bulk deformation during F_2-folding, (ii) with $P_{(0)} = 90°$ and (iii) Z-axis always coinciding with L_1 at the hinge of F_2, (iv) while the F_2 axis is parallel neither to X nor to Y and (v) $\lambda_1 \neq \lambda_2$. With other conditions remaining the same, the variation in $L_1 \wedge F_2$ over a fold would be greatest if the F_2 axis was initially at 45° to X (Figs. 4j–l). At the point of inflection of a fold, $L_1 \wedge F_2$ would change very slowly with progressive deformation if the F_2 axis was initially close to either X or Y (Fig. 6). Hence, unless the total shortening was exceptionally high, a strongly curved type 4 pattern would indicate that the F_2 axis was initially neither close to X nor close to Y and that $\lambda_1 \gg \lambda_2$. Nevertheless, a strongly curved type 4 pattern on the unrolled form surface and with very low values of $L_1 \wedge F_2$ at the limbs (Fig. 3) does indicate that the stretching along the fold axis is quite large and that in its final position F_2 makes a small angle with X.

The type 2(a) pattern also develops under rather restricted conditions. Its rotational symmetry generally develops when $0 < P_{(0)} < 90°$ and the two limbs of the fold are symmetrically oriented with respect to the principal axes of bulk strain. This implies that the bulk deformation is coaxial, with F_2 parallel to either X or Y (Figs. 4a & b and 5). In certain cases L_1 at the hinge makes a small or moderate angle with the F_2 axis while on the limb L_1 is nearly at right angles to the F_2 axis. Such a pattern can develop only if the F_2 axis is parallel to Y and $\lambda_1 \gg \lambda_2$. When $\lambda_1 = \lambda_2$, the 2(a) pattern can develop at all values of ψ.

The type 2(b) pattern forms under a wide range of ψ and $P_{(0)}$ (Fig. 5). The asymmetry of the pattern is shown by dissimilar values of $L_1 \wedge F_2$ at the two inflection points of the fold. The 2(b) patterns which show small values of $L_1 \wedge F_2$ at both the hinge and the limbs (Fig. 4c) develop when both ψ and $P_{(0)}$ are small. This particular pattern does not change to other types with progressive deformation. Hence the occurrence of this pattern over tight folds indicates that the F_2 axis was close to X and that the initial angle between L_1 and the F_2 axis was small. 2(b) patterns as in Fig. 4(d) can develop only if the F_2 axis is initially close to Y. However, this pattern can

form in a wide range of $P_{(0)}$ but not at values close to 90°. Nevertheless, if $P_{(0)}$ is small the pattern will not evolve into type 2(c), unless the total deformation is exceptionally high. In other situations, the 2(b) pattern which is most likely to be encountered is shown in Fig. 4(e), with small $L_1 \wedge F_2$ and a small curvature of L_1 on one limb and with large $L_1 \wedge F_2$ and a large curvature of L_1 on the other limb. These are the patterns which may commonly evolve into type 2(c) with progressive deformation (Fig. 4f).

Types 3(a) and 3(b) patterns occupy a relatively small field in a ψ-$P_{(0)}$ diagram. They develop under the condition of very large $P_{(0)}$ (close to 90°) and within a range of intermediate to large ψ. Over this entire field a 3(a) pattern will change to 3(b) with progressive deformation (Figs. 4h & i); however a *strongly bent* 3(b) pattern would commonly develop when ψ has only intermediate values (Fig. 4i). Hence in areas where an exceptionally large deformation is not expected, the occurrence of a strongly curved 3(b) pattern on the unrolled form surface implies that $P_{(0)}$ was very close to 90° and the initial F_2 axis was neither close to X nor close to Y.

Types 5 and 6 patterns did not develop in any situation of our theoretical models. They are also rather rare in nature. Excepting a single exposure in Jhamarkotra in Rajasthan, we did not find the type 5 pattern. Ramsay (1967, p. 464) interpreted this pattern by tangential longitudinal strain over the outer arc of a folded layer. Though rare, the type 6 pattern was found in some places in Central Rajasthan. The mode of development of this pattern is discussed separately.

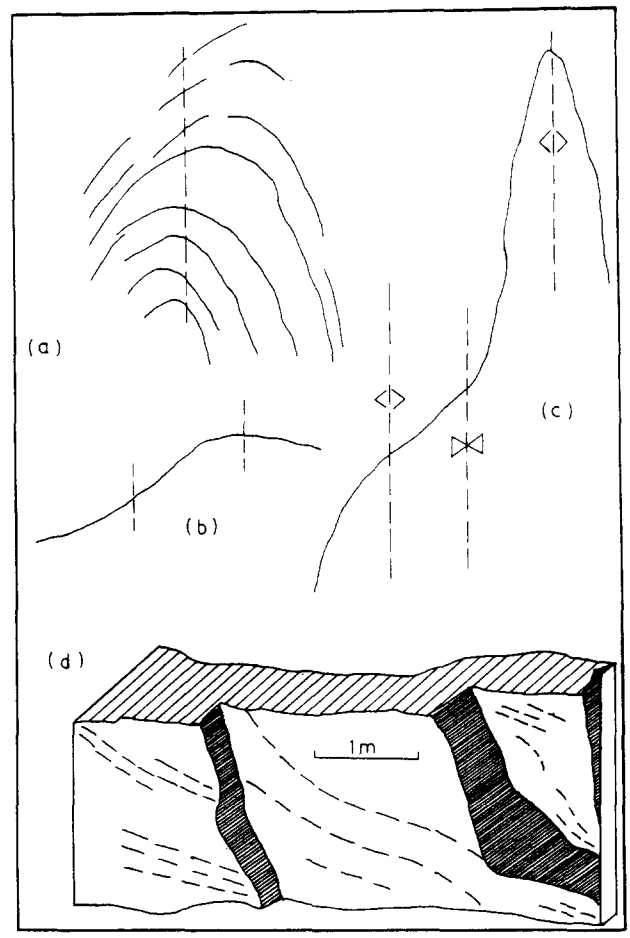

Fig. 7. Some natural lineation patterns on unrolled form surfaces. (a) Complex pattern, Aravalli schist, Central Rajasthan. The F_2 fold is nearly isoclinal. Note that $L_1 \wedge F_2$ is variable along the fold axis. Along the hinge (dashed line) the variation of $L_1 \wedge F_2$ *is more than* 90°. (b) Dissimilar lineation patterns in congruent folds, Bhindar, Rajasthan. 3(b) pattern on a tight fold (right) and 3(a) pattern on an open subsidiary fold (left). (c) Strongly curved type 4 pattern on upright very tight fold (right) and much more gently curved 3(a) patterns on open congruent subsidiary folds (left) on one limb of the tight fold. Fuchsite quartzite about 6 km from Hosdurga on Ajjampur–Hosdurga road, Karnataka. (d) Curved lineation on essentially planar vertical foliation in amphibolites. Railway cutting, south of Jasidih railway station, Bihar.

DEVELOPMENT OF COMPLEX LINEATION PATTERNS

In the type 6 pattern (Fig. 7a), unlike other types, $L_1 \wedge F_2$ does not remain constant along a line parallel to the fold axis. Such a pattern cannot develop according to our theoretical model in which the fold axis always lies on the XY plane and the rotating fold hinge continues to coincide with a single material line. In other situations, in which the enveloping surface is not parallel to any of the principal axes of strain or in situations of non-coaxial bulk deformation, the fold hinge may shift its position by sweeping through different material lines (Ramberg & Ghosh 1977, pp. 323–324). In such circumstances the successive positions of a fold hinge may or may not remain parallel. If the successive positions of the hinge do not remain parallel, $L_1 \wedge F_2$ can vary not only at different values of the dip angle α but also along lines α = constant (Fig. 8). No doubt a type 6 pattern may also develop if L_1 is initially curved, that is if F_1 is initially non-cylindrical. However, there are certain geometrical peculiarities common to all the type 6 patterns observed by us in the Aravalli schists of Central Rajasthan. (1) They are clearly recognizable on tight or isoclinal F_2-folds. While $L_1 \wedge F_2$ on such folds shows a wide range of variation (sometimes through more than 90°) along lines parallel to the F_2 axis in the neighbourhood of the hinge,

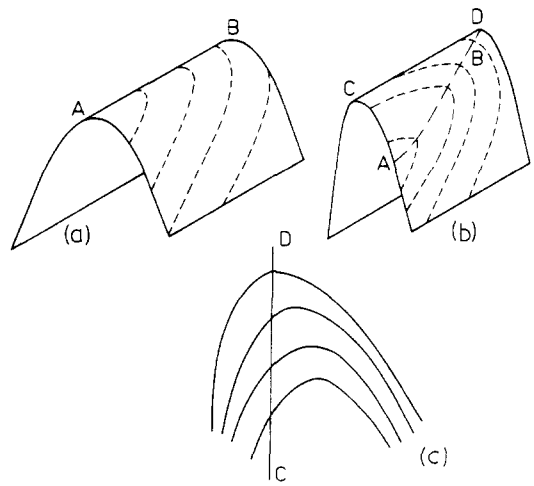

Fig. 8. Development of type 6 pattern by rotation of hinge line through successive material lines. (a) Development of type 4 or 3(b) pattern with AB as hinge. (b) At a subsequent stage the geometrically defined new hinge line is CD. Earlier pattern is modified with $L_1 \wedge F_2$ varying along lines parallel to CD. (c) Pattern of L_1 after the fold is unrolled around CD.

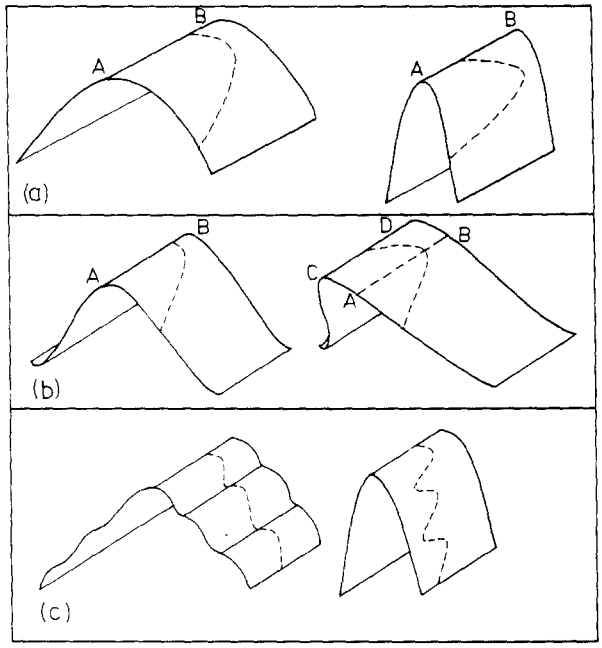

Fig. 9. Three alternative ways of developing curved lineations on essentially planar surfaces by (a) tightening of fold so that a curved segment of L_1 is shifted from near hinge zone to limb, (b) shifting of hinge line parallel to itself during progressive increase in the asymmetry of fold and (c) flattening out of subsidiary folds on the limbs of a main fold during its progressive tightening.

$L_1 \wedge F_2$ along the flanks of the folds is consistently small and shows a small range of variation. (2) The sense of closure of the curved lineation is always the same throughout the unrolled form surface of any one of these folds in the mesoscopic scale. This would suggest that, for these examples, the type 6 pattern did not develop by folding of an initially curved L_1. The occurrence of type 6 patterns in the Aravalli schists would then imply that the planar segments of the isoclinal F_1 folds were locally strongly oblique to all the principal axes of strain during the F_2-deformation.

CURVED LINEATIONS ON PLANAR SURFACES

In shear zones, a curved lineation on a planar surface may develop in a single deformation by a mechanism similar to that of sheath folding, as proposed by Ramsay (1980). From the foregoing analysis it is apparent that in some other situations a curved lineation on a more or less planar surface (Fig. 7d) may develop by any one of the following processes. (1) In all the patterns from types 2–4, the lineation remains curved on the unrolled fold-limbs. With progressive deformation this curvature may be accentuated while the fold limb may gradually approach a more or less planar form. Since in all such cases, the maximum curvature of the deformed lineation will be fairly close to the hinge zone (Fig. 9a), this mechanism can give rise to a strongly curved L_1 on the fold limb only if the deformation is exceptionally large. (2) However, if the hinge line sweeps through different material lines, either parallel to earlier orientations or at an angle with them, a strongly curved pattern near an earlier hinge may later be shifted to the straight segment of a limb (Fig. 9b). (3) A smaller congruent fold on the limb of a larger fold may show a strong curvature near its hinge. If during the tightening of the larger fold, the smaller fold on the limb is unrolled or flattened out, we may then obtain a strongly curved lineation on the flattened out limb of the larger fold (Fig. 9c).

SEQUENCE OF SMALL AND LARGE FOLDS

Congruent small folds on limbs of larger folds are usually interpreted to have been initiated either at the same time as the larger fold or at a slightly earlier stage (Ramberg 1964, Ghosh 1968, pp. 226–228). Hence, it came to us as a surprise when the lineation patterns in certain outcrops gave definite evidence that the smaller folds on the limbs were initiated when the larger fold was already quite mature. In all such cases the early lineation deformed over a tight larger fold is strongly curved and of type 4 or type 3(b), indicating that the lineation initially made an angle of 90° or almost 90° with the later fold axis. The patterns of deformed lineations on the more open subsidiary folds on the same form surface indicate that the smaller folds were initiated when the angle between the lineation and the fold axis of the larger fold had been considerably reduced. That is why the lineation on these subsidiary folds is weakly curved and of type 2(b) or 3(a) (Figs. 7b & c). In other words the lineation of type 4 or 3(b) over the larger fold must have had a fairly strong curvature, and hence the fold must have acquired at least a moderately large amplitude, before the congruent subsidiary folds were initiated on its limb. A similar mechanism was proposed by Mukhopadhyay & Ghosh (1980, p. 73) to explain the simultaneous occurrence of different types of lineation patterns among the mesoscopic folds of an area. The mechanism of development of such late subsidiary folds is not clearly understood. The observations nevertheless do indicate that congruent subsidiary folds may be initiated when the major fold is already quite mature.

STRUCTURAL SIGNIFICANCE OF DEFORMED LINEATION PATTERNS IN CENTRAL RAJASTHAN

We indicated earlier that in the Banded Gneissic Complex and the Aravalli rocks of Central Rajasthan the bulk deformation during F_2-folding was essentially coaxial, with the Z-axis subhorizontal and having an E–ESE trend. The occurrence of type 3(b) and type 4 patterns of L_1, along with the high angles between L_1 and F_2 in the majority of type 1 patterns, indicate further that on average the F_2 axis was initially nearly at right angles to L_1. Hence L_1 must have been initially very close to Z.

We can also have a rough idea about the plunge of the X-axis in the N–NNE-striking subvertical axial surface of F_2. A review of the existing literature (Naha 1983) shows that in spite of a large range of plunge the majority

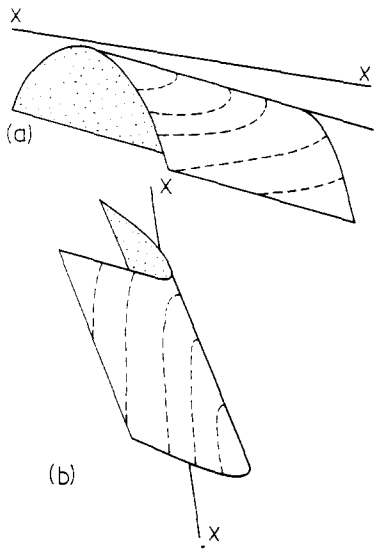

Fig. 10. Sense of curvature of type 4 or type 3(b) patterns. (a) F_2 steeper than X-axis of bulk strain. In this case the deformed L_1 shows a closure towards plunge direction over an antiform. (b) X-axis steeper than the F_2 axis. Deformed L_1 closes against plunge of F_2 antiform.

of F_2 hinges have a low to moderate plunge to the N or S. Consider two alternative cases: (1) the plunge of the X-axis was gentler than that of the initial F_2 axis and (2) X had a steeper plunge than the initial F_2 axis. In either case we would get a type 3(b) or 4 pattern of deformed L_1 if the initial angle between L_1 and F_2 was close to 90°. The numerical computations of our empirical model indicate that the sense of curvature of the deformed lineation would be different in the two cases. In the first case the closure of the bent L_1 would be down the plunge of antiforms (Fig. 10a) and against the plunge of synforms. In the second case the closure would be against the plunge of antiforms (Fig. 10b) and towards the plunge of synforms. In all the cases where we found patterns of type 3(b) or type 4 in Central Rajasthan the closure of L_1 was down the plunge of antiforms and against the plunge of synforms. Hence the X-axis of bulk strain must have had a gentler plunge than that of the initial F_2 axis. Moreover, since our theoretical analysis has shown that under usual circumstances (i.e. if the deformation is not exceptionally large) a strongly curved type 3(b) or type 4 lineation cannot develop when the initial angle between X and the F_2 axis is close to 0 or 90°, the X-axis must have made a moderately large angle with the initial F_2. Hence the X-axis of bulk strain must have been either subhorizontal or gently plunging and with a N–NNE trend.

It is noteworthy that similar differences in the sense of curvature of the lineation patterns over antiforms and synforms were first interpreted by Hudleston (1973a, pp. 128–129) from the Monar area of Scotland, and our interpretation, following from the numerical models, is very similar to that given by him.

SUMMARY AND CONCLUSIONS

(1) All types of lineation patterns excepting types 5 and 6 were obtained from the numerical solutions of the model of simultaneous buckling and flattening. However, not all of them are equally informative. The results suggest that the 2(a) pattern is characteristic of progressive coaxial bulk deformation. However, since in our model it formed under rather restricted situations, namely when the F_2 axis is parallel to either X or Y, or when $\lambda_1 = \lambda_2$, its occurrence is likely to be rare. The 2(b) pattern, which develops under a wide range of ψ and $P_{(0)}$ is fairly common. A 2(b) pattern can be useful in two cases. (i) If $L_1 \wedge F_2$ is low at both the hinge and the limbs (Fig. 4c) we may conclude that both ψ and $P_{(0)}$ were low. (ii) If $L_1 \wedge F_2$ is low at the hinge and rather high at the limbs (Fig. 4d), the pattern would indicate that the F_2 axis was initially close to Y. A strongly curved 2(c) pattern (Fig. 4f) develops only when ψ is moderately large and $P_{(0)}$ is large but not close to 90°. The 3(a) pattern develops over a wide range of ψ but is characteristic of situations with large values of $P_{(0)}$ (Fig. 4g). The presence of a strongly curved 3(b) pattern indicates that $P_{(0)}$ was close to 90°, ψ had an intermediate value and λ_1 was considerably greater than λ_2.

(2) A type 4 pattern, or a 3(b) pattern which closely approximates type 4, is fairly common in certain regions and has considerable structural importance. The occurrence of this type of lineation pattern indicates that the bulk deformation was essentially coaxial, the early lineation was initially almost perpendicular to the late fold axis, the Z-axis of bulk strain during F_2-folding was very close to the initial orientation of L_1 and that λ_1 was considerably greater than λ_2. Moreover, from the occurrence of a strongly curved lineation on an unrolled form surface and from the sense of curvature of the lineation over antiforms and synforms, we can have an approximate idea about the orientation of the X-axis of bulk strain. In the majority of our natural examples where a type 4 pattern was observed, the lineation did not lie on a plane. The occurrence of a type 4 pattern, in such cases, is particularly informative since it implies that the late fold is neither a shear fold nor a parallel fold modified by flattening.

(3) The lineation patterns in an area are often an association of different types. As pointed out by Mukhopadhyay & Ghosh (1980) such an association may occur because of the different amounts of initial homogeneous strain undergone by rocks of different competences and/or because of the non-synchronous development of small folds at different parts of a larger fold. In all such cases the dissimilar patterns developed because of the different values of $L_1 \wedge F_2$ during the initiation of the folds. The present study indicates that dissimilar lineation patterns may also be associated because of a variation in the initial attitude of the F_2 axis with respect to the bulk strain axes and because of a spatial variation in the intensity of deformation. With increasing deformation one lineation pattern may change over to another. Hence with varying intensities of deformation the different members of each transitional series 2(b) → 2(c), 3(a) → 2(b) → 2(c) and 3(a) → 3(b) may occur in the same area. The occurrence of dissimilar lineation patterns on the

main fold and coaxial subsidiary folds of a single form surface is particularly significant since it enables us to determine the sequence of folding in a single progressive deformation.

(4) The effect of tangential longitudinal strain was disregarded in our theoretical model. Hence the results of the present analysis are valid when the homogeneous strain is large in comparison with the tangential longitudinal strain. A deformed lineation on a fold produced by tangential longitudinal strain will tend to form a 2(a) pattern on the inner surface and 5(a) pattern on the outer surface of a folded layer. Since 5(a) and 5(b) patterns are very rarely observed among natural examples, we suggest that the variation in $L_1 \wedge F_2$ produced by tangential longitudinal strain is rather small, so that it either remains unnoticed or is easily masked by the larger contribution of homogeneous strain.

(5) In our theoretical model we assumed that (i) the folded surface in transverse profile is represented by a sine curve, (ii) the bulk deformation is coaxial and (iii) the layer is initially parallel to the Z-direction of bulk strain. For a sinusoidal fold the ratio of hinge zone to limb becomes very small when the interlimb angle of the fold is greatly reduced. As a consequence the greatest change in $L_1 \wedge F_2$ takes place within a very narrow zone near the hinge line. If a non-sinusoidal F_2-fold is nearly isoclinal but has a broad hinge zone, the lineation of the unrolled form surface will be less sharply bent and the point of maximum curvature will not necessarily lie close to the hinge line; otherwise the type of lineation pattern will be the same as on a sinusoidally folded surface. If the second or the third condition is not satisfied the fold limbs will not maintain symmetrical orientations with respect to the principal axes of bulk strain and hence patterns of types 2(a) and 4 will not develop. If the bulk deformation is coaxial but the layer is at a low angle to the Z-axis, the fields of dissimilar lineation patterns will still be essentially the same as shown in Fig. 5, or only marginally modified. It is more difficult to predict the types of lineation pattern expected in progressive non-coaxial deformation. However, for non-coaxial deformations whose instantaneous character does not change with time, a 3(b) or 2(c) pattern will develop only when $P_{(0)}$ is very large. On the other hand a low value of $P_{(0)}$ will generally give rise to 2(b) patterns. Further, a type 6 pattern may develop when the second or the third condition is not satisfied. Recognition of this pattern is of considerable theoretical importance, since it may give us the rare opportunity of confirming that the hinge line of a fold rotated through successive material lines in the course of progressive deformation.

(6) The curving of an early lineation on a more or less planar segment of a foliation surface may be explained in different ways. A likely process is a shifting of zones of strong variation of $L_1 \wedge F_2$ from the hinge zone to the essentially planar segment of a limb, either by a progressive tightening of the fold or by a migration of the geometrically defined hinge line over successive material lines.

REFERENCES

Belyakov, V. M., Kavtsova, P. I. & Rappopart, M. G. 1965. *Tables of Elliptic Integrals. Part I.* Pergamon Press, Oxford.

Biot, M. A. 1965. *Mechanics of Incremental Deformations.* Wiley, New York.

Dutta, M. & Debnath, L. 1965. *Elements of the Theory of Elliptic and Associated Functions with Applications.* The World Press Private, Calcutta.

Ghosh, S. K. 1968. Experiments of buckling of multilayers which permit inter-layer gliding. *Tectonophysics* **6**, 207–249.

Hancock, H. 1958. *Elliptic Integrals.* Dover, New York.

Hobbs, B. E., Means, W. D. & Williams, P. F. 1976. *An Outline of Structural Geology.* Wiley, New York.

Hudleston, P. J. 1973a. The analysis and interpretation of minor folds developed in the Moine rocks of Monar, Scotland. *Tectonophysics* **17**, 89–132.

Hudleston, P. J. 1973b. Fold morphology and some geometrical implications of theories of fold development. *Tectonophysics* **16**, 1–46.

Mukhopadhyay, D. & Ghosh, K. P. 1980. Deformation of early lineation in the Aravalli rocks near Fatehpur, Udaipur district, southern Rajasthan, India. *Ind. J. Earth Sci.* **7**, 64–75.

Naha, K. 1983. Structural–stratigraphic relations of the pre-Delhi rocks of south-central Rajasthan: a summary. In: *Structure and Tectonics of Precambrian Rocks of India* (edited by Sinha Roy, S.) Hindustan Publishing Corporation (India), Delhi, 40–52.

Naha, K. & Halyburton, R. V. 1977a. Structural pattern and strain history of a superposed fold system in the Precambrian of central Rajasthan, India. II. Strain History. *Precambrian Res.* **4**, 85–111.

Naha, K. & Halyburton, R. V. 1977b. Structural pattern and strain history of a superposed fold system in the Precambrian of central Rajasthan, India. I. Structural pattern in the "Main Raialo syncline", Central Rajasthan. *Precambrian Res.* **4**, 39–84.

Narayan, S. 1968. *A Text Book of Cartesian Tensors.* S. Chand, Delhi.

Peirce, B. O. 1956. *A Short Table of Integrals.* (Fourth Edn). Blaisdell, New York.

Ramberg, H. 1964. Selective buckling of composite layers with contrasted rheological properties, a theory for simultaneous formation of several orders of folds. *Tectonophysics* **1**, 307–341.

Ramberg, H. & Ghosh, S. K. 1977. Rotation and strain of linear and planar structures in three-dimensional progressive deformation. *Tectonophysics* **40**, 309–337.

Ramsay, J. G. 1960. The deformation of early linear structures in areas of repeated folding. *J. Geol.* **68**, 75–93.

Ramsay, J. G. 1967. *Folding and Fracturing of Rocks.* McGraw-Hill, New York.

Ramsay, J. G. 1980. Shear zone geometry: a review. *J. Struct. Geol.* **2**, 83–99.

Roy, A. B. & Jain, A. K. 1974. Polyphase deformation in the lead–zinc bearing Precambrian rocks of Zawarmala, District Udaipur, southern Rajasthan. *Q. Jl Geol. Min. met. Soc. Ind.*, Golden Jubilee vol.

Roy, A. B., Somani, M. K. & Sharma, N. K. 1981. Aravalli–Pre-Aravalli relationship: a study from the Bhindar region, southern Rajasthan. *Ind. J. Earth Sci.* **8**, 119–130.

Spenceley, G. W. & Spenceley, R. M. 1947. Smithsonian Elliptic Functions Tables. Smithsonian Miscellaneous Collections **109**. The Smithsonian Institution, Washington D.C.

APPENDIX

Notation

In the following analysis the planar structure, the early lineation and the later fold axis will be denoted by S, L and F, respectively. The angle between L and F will be denoted by P. In the undeformed state they will be represented by the subscript zero within parentheses while in the deformed state in successive increments (step 1, step 2, etc.) the corresponding entities will be designated by the subscripts 1, 2, etc. in parentheses. Thus, $l_{(1S)i}$ and $l_{(1L)i}$, $(i = 1, 2, 3)$, are the direction cosines of the S-pole and L at the points of inflection at step 1, $l'_{(1S)i}$ and $l'_{(1L)i}$ are the corresponding direction cosines at points intermediate between the inflection point and the hinge point and $h_{(2S)i}$ and $h_{(2L)i}$ are the direction cosines of S and L at the hinge at step 2. α and α' are the dip angles (with reference to the hinge) at the point of inflection and at an intermediate point. $\lambda_{(H)i}$ and λ_i are the quadratic elongations during initial homogeneous strain and incremental homogeneous strain,

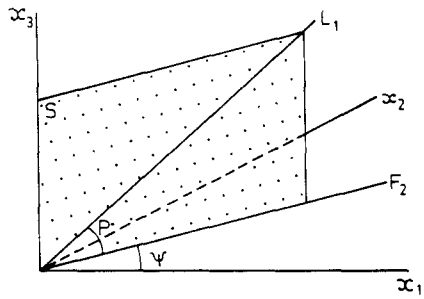

Fig. 11. Orientation of S (stippled), L and F with respect to the coordinate axes. $P = L_1 \wedge F_2$. ψ = initial angle between x_1 and F_2. Note that F_2 lies on the x_1x_2-plane.

respectively. We have chosen the coordinate axes x_1, x_2 and x_3 parallel to the X, Y and Z axes of bulk strain during the development of the later fold. The acute angle between the x_1 axis and the trace of $S_{(0)}$ on the x_1x_2-plane will be designated by ψ. a and b are the amplitude and quarter wavelength of the sine curve.

Step 1: initial homogeneous strain

If $P_{(0)}$ is the angle between $L_{(0)}$ and the trace of $S_{(0)}$ on the x_1x_2-plane (Fig. 11), the direction cosines of $L_{(0)}$ are:

$$l_{(0L)1} = \frac{-1}{\sqrt{1 - l^2_{(0S)3}}}\,[l_{(0S)1}l_{(0S)3}\sin P_{(0)} + l_{(0S)2}\cos P_{(0)}],$$

$$l_{(0L)2} = \frac{1}{\sqrt{1 - l^2_{(0S)3}}}\,[l_{(0S)1}\cos P_{(0)} - l_{(0S)3}l_{(0S)2}\sin P_{(0)}],$$

and

$$l_{(0L)3} = \sqrt{1 - l^2_{(0S)3}}\,\sin P_{(0)}. \tag{3}$$

After initial homogeneous strain $S_{(0)}$ is changed to $S_{(1)}$. The direction cosines of its normal are

$$l_{(1S)i} = \frac{l_{(0S)i}/\sqrt{\lambda_{(H)i}}}{\delta_1}, \tag{4a}$$

where

$$\delta_1 = \left[\sum_{i=1}^{3} \frac{l^2_{(0S)i}}{\lambda_{(H)i}}\right]^{1/2}, \tag{4b}$$

and the direction cosines of $L_{(1)}$ are

$$l_{(1L)i} = \frac{l_{(0L)i}\sqrt{\lambda_{(H)i}}}{\delta_2}, \tag{5a}$$

where

$$\delta_2 = \left[\sum_{i=1}^{3} l^2_{(0L)i}\lambda_{(H)i}\right]^{1/2}. \tag{5b}$$

The direction cosines of the fold axis will be given by those of the trace of $S_{(1)}$ on the x_1x_2-plane

$$l_{(1F)1} = \frac{-l_{(1S)2}}{\sqrt{1 - l^2_{(1S)3}}},$$

$$l_{(1F)2} = \frac{l_{(1S)1}}{\sqrt{1 - l^2_{(1S)3}}},$$

and

$$l_{(1F)3} = 0. \tag{6}$$

The angle between $L_{(1)}$ and $F_{(1)}$ is

$$P_{(1)} = \cos^{-1}\left[\sum_{i=1}^{3} l_{(1L)i}l_{(1F)i}\right]. \tag{7}$$

Step 2: initial buckling

Structural elements at points of inflection. During the initial buckling the planar segment is deformed into a cylindrical fold, with the middle surface appearing as a sine curve on the profile plane. If $\Delta\alpha$ is the amount of rotation at a point of inflection, the direction cosines of the normal to the tangent at that point and of the lineation are respectively

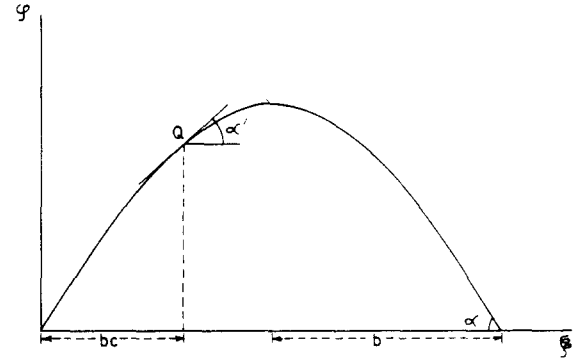

Fig. 12. Trace of middle surface of folded layer on the profile plane. ξ is parallel to the x_3 axis. α is the dip angle at the point of inflection and α' is the dip angle at a point Q with ξ coordinate as bc. b is the quarter wavelength.

$$l_{(2S)i} = c_{ij}l_{(1S)j}, \tag{8}$$

and

$$l_{(2L)i} = c_{ij}l_{(1L)j}, \tag{9}$$

with summation over the repeated suffix. Here

$$c_{ij} = \cos(\Delta\alpha)\delta_{ij} + (1 - \cos\Delta\alpha)l_{(1F)i}l_{(1F)j} - \sin(\Delta\alpha)\varepsilon_{ijk}l_{(1F)k} \tag{10}$$

(Narayan 1968, p. 70) and δ_{ij} and ε_{ijk} are respectively the Kronecker tensor and the alternate tensor. (δ_{ij} is 0 if $i \neq j$ and is 1 if $i = j$. $\varepsilon_{ijk} = 0$ if any two of i, j, k are equal. $\varepsilon_{ijk} = 1$ or -1 depending on whether ijk is a cyclic or anticyclic permutation of 1, 2, 3.) Positive and negative values of $\Delta\alpha$ give the orientations of $S_{(1)}$ and $L_{(1)}$ at the two points of inflection. In the numerical calculations $\Delta\alpha$ was taken as 1 and $-1°$. The angle between the lineation and fold axis, as given by eqn. (7), remains unchanged, so that $P_{(2)} = P_{(1)}$.

Structural elements at points intermediate between the inflection and hinge points. The profile plane in our theoretical model always remains parallel to the x_3-axis. We have chosen the coordinate axes ξ, ζ on this plane with ξ parallel to x_3. The trace of the folded middle surface of the layer is then given by the equation

$$\zeta = a\sin(n\xi) \tag{11}$$

where $n = 2\pi/4b$, b being the quarter wavelength. Let Q be a point on this curve after the stage of initial buckling (Fig. 12) and let its ξ-coordinate on the profile plane be bc, so that by varying the value of c between 1 and 0, we can locate any point on the fold profile. If α' be the dip angle at Q, then from eqn. (11) we find

$$\tan\alpha' = \frac{d\zeta}{d\xi} = an\cos(n\xi).$$

At $\xi = 0$,

$$\frac{d\zeta}{d\xi} = \tan(\Delta\alpha) = an.$$

Hence

$$\tan\alpha' = \tan(\Delta\alpha)\cos\left(\frac{\pi}{2}c\right), \tag{12}$$

where $\Delta\alpha$ is the dip angle at the point of inflection. To find the direction cosines of the normal to S at Q, we use an equation similar to (6) and obtain the following relations

$$l'_{(2S)1} = l_{(1F)2}\sqrt{1 - \{l'_{(2S)3}\}^2},$$

$$l'_{(2S)1} = -l_{(1F)2}\sqrt{1 - \{l'_{(2S)3}\}^2},$$

and

$$l'_{(2S)3} = \pm\sin\alpha'. \tag{13}$$

The direction cosines of $L_{(2)}$ at the same point are obtained by using

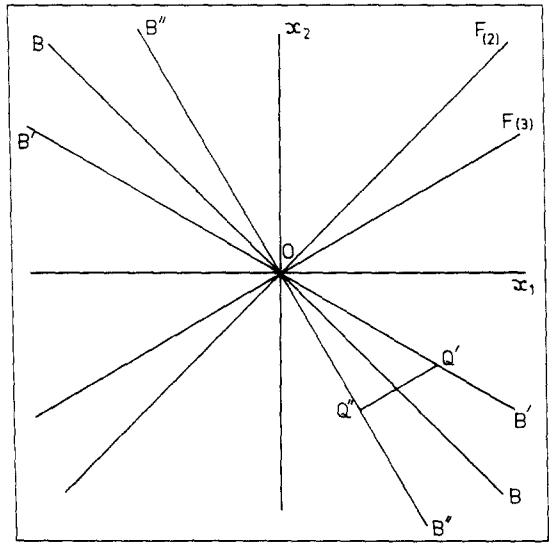

Fig. 13. Traces of B, B' and B'' planes on the x_1x_2 plane. B is the geometrically defined profile plane of the fold at step 2. After incremental homogeneous strain (step 3) the fold axis has changed to position $F_{(3)}$ while B has deformed as a material plane to B'. B'' is the geometrically defined profile plane for $F_{(3)}$. A point Q' on the B' plane is projected parallel to $F_{(3)}$ on B'' plane. Here $0Q' = \zeta'$, $0Q'' = \zeta'' = \zeta' \cos(\angle Q'0Q'') = \zeta' \sin(F_{(3)} \wedge B')$.

eqn. (3) after replacing l by l', $P_{(0)}$ by $P_{(2)}$ and by replacing the subscript 0 by the subscript 2 within parentheses. For instance

$$l'_{(2L)3} = \sqrt{1 - \{l'_{(2S)3}\}^2} \sin P_{(2)}, \tag{14}$$

where $P_{(2)}$ is given by eqn. (7) and by the relation $P_{(2)} = P_{(1)}$. Note that at this stage the angle between the lineation and the fold axis is the same at all points.

Step 3: incremental homogeneous strain

Structural elements at the points of inflection. Let $\Delta\varepsilon_i$ be the increment of homogeneous strain along x_i and the principal quadratic elongations be $\lambda_i = (1 + \Delta\varepsilon_i)$.[2] The direction cosines, $l_{(3S)i}$, of the normal to S are obtained from eqn. (4) by replacing $l_{(1S)i}$ by $l_{(3S)i}$, $l_{(0S)i}$ by $l_{(2S)i}$ and $\lambda_{(H)i}$ by λ_i. The direction cosines of the lineation are similarly obtained from eqn. (5) by replacing $l_{(1L)i}$ by $l_{(3L)i}$, $l_{(0L)i}$ by $l_{(2L)i}$ and $\lambda_{(H)i}$ by λ_i. The direction cosines of the fold axis are obtained from eqn. (6) by replacing $l_{(1F)i}$ by $l_{(3F)i}$ and $l_{(1S)i}$ by $l_{(3S)i}$. The angle between the fold axis and the lineation at the point of inflection is given by the relation

$$P_{(3)} = \cos^{-1}[l_{(3L)i} \cdot l_{(3F)i}], \tag{15}$$

with summation over the repeated suffix i.

Structural elements at points between the inflection and hinge points. Let $F_{(2)}$ be the fold axis at step 2. On its profile plane (say, plane B) the trace of the folded surface appears as a sine curve $\zeta = a \sin(n\xi)$. During incremental homogeneous strain $F_{(2)}$ changes to $F_{(3)}$; its geometrically defined profile plane (say, plane B'') would no longer coincide with the material plane B' obtained by deformation of B (Fig. 13). It can be shown that the sine curve $\zeta = a \sin(n\xi)$ of plane B is deformed to a sine curve $\zeta' = a' \sin(n'\xi')$ on plane B', where $a' = a\sqrt{\lambda}$ and $n' = n/\sqrt{\lambda_3}$, λ being the quadratic elongation along the trace of B' on the x_1x_2 plane. Moreover, if the curve on B' is projected along the fold axis on the profile plane B'', it still remains a sine curve $\zeta'' = a'' \sin(n''\xi'')$, where $a'' = a' \sin[F_{(3)} \wedge B']$ (Fig. 14), and $n'' = n'$. Because of the incremental homogeneous strain, the position of point Q (with ξ-coordinate $= bc$) on the sine curve on plane B changes to Q' (with the ξ-coordinate $b'c'$) on the B' plane. Since $b'/b = b'c'/bc = \sqrt{\lambda}_3$, we have $c' = c$. Again, since Q' is projected along the fold axis (Fig. 14) on the B'' plane, the ξ-coordinate of Q' remains unchanged, so that $b'' = b'$ and $c'' = c'$. Knowing the quarter wavelength b'' and the c-value (c''), we can now locate Q'' on the profile plane. The dip angle at this point is found from eqn. (12)

$$\tan\alpha' = \tan\alpha \cdot \cos\left(\frac{\pi}{2} \cdot c''\right). \tag{16}$$

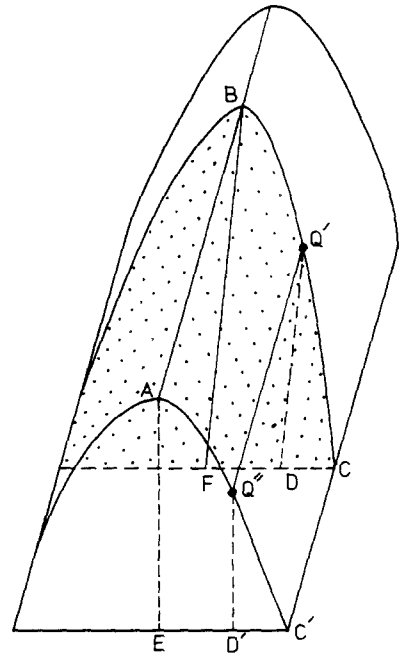

Fig. 14. The projection of the point Q' on the B' plane (stippled) along the fold axis to Q'' on the B'' plane. The ξ coordinate of Q' is CD and that of Q'' is C'D'. CD = C'D', so that the ξ coordinates of the two points are the same. BF = a' and AE = a''. Hence $a'' = \text{BF} \sin(\angle\text{ABF})$.

The direction cosines of the normal to the S-surface are given by relations similar to eqn. (13)

$$l'_{(3S)3} = \pm\sin\alpha',$$

$$l'_{(3S)2} = -l_{(3F)1}\sqrt{1 - \{l'_{(3S)3}\}^2},$$

and

$$l'_{(3S)1} = l_{(3F)2}\sqrt{1 - \{l'_{(3S)3}\}^2}. \tag{17a}$$

Alternatively, from eqn. (16) and from the relation $l'_{(3S)3} = \pm\sin\alpha'$, we may obtain $l'_{(3S)3}$ directly in terms of α

$$l'_{(3S)3} = \left[1 - \frac{1}{1 + \tan^2\alpha \cos^2\left(\frac{\pi}{2} c''\right)}\right]^{1/2}. \tag{17b}$$

The sign of $l'_{(3S)3}$ should be the same as that of $l_{(3S)3}$. The direction cosines of L at Q'' are obtained from eqn. (5) by replacing $l_{(1L)i}$ by $l'_{(3L)i}$, $l_{(0L)i}$ by $l'_{(2L)i}$ and $\lambda_{(H)i}$ by λ_i. The angle between the lineation and the fold axis at Q'' is

$$P'_{(3)} = \cos^{-1}[l'_{(3L)i} l_{(3F)i}]. \tag{18}$$

Structural elements at the hinge. The direction cosines $h_{(3S)i}$ and $h_{(3L)i}$ of S and L at the hinge are

$$h_{(3S)i} = \frac{h_{(1S)i}}{\sqrt{\lambda_i}\,\delta}, \tag{19}$$

where

$$\delta = \left[\sum_{i=1}^{3} \frac{h^2_{(1S)i}}{\lambda_i}\right]^{1/2},$$

and

$$h_{(3L)i} = \frac{h_{(1L)i}\sqrt{\lambda_i}}{\delta'}, \tag{20}$$

with

$$\delta' = \left[\sum_{i=1}^{3} h^2_{(1L)i}\lambda_i\right]^{1/2},$$

where $h_{(1S)i} \equiv l_{(1S)i}$ and $h_{(1L)i} \equiv l_{(1L)i}$ and are obtained from eqns. (4) and (5). The angle between the fold axis and the lineation at the hinge is obtained from eqn. (18) by replacing l' by h' on the right-hand side.

Step 4: incremental buckling

Structural elements at points of inflection. Our first objective at this stage is to determine the amount of rigid rotation at the point of inflection of the fold when the wavelength of the sine curve changes by a known small amount but while the length of arc remains constant. Let the fold profile at the end of step 3 be represented by the equation $\zeta = a \sin(n\xi)$ where $n = 2\pi/4b$, b being the quarter wavelength. The arc-length of the sine curve is

$$s = \int_0^{\xi} \sqrt{1 + \left(\frac{d\zeta}{d\xi}\right)^2}\, d\xi. \tag{21}$$

With $n\xi = z$, the integral can be represented as an elliptic integral:

$$s = \frac{\sqrt{1 + a^2n^2}}{n} \int_0^z \sqrt{1 - k^2 \sin^2 z}\, dz,$$

where

$$k^2 = \frac{a^2n^2}{1 + a^2n^2}$$

or,

$$s = \frac{1}{n} \sqrt{1 + a^2n^2}\, E(k, z), \tag{22}$$

where $E(k, z)$ is an elliptic integral of the second kind (Hancock 1958, Dutta & Debnath 1965). Since $d\zeta/d\xi = an \cos(n\xi)$, we have for the point of inflection $\xi = 0$,

$$\tan\alpha = an. \tag{23a}$$

Therefore,

$$k^2 = \frac{a^2n^2}{1 + a^2n^2} = \sin^2\alpha. \tag{23b}$$

Equation (22) can then be written as

$$s = \frac{2bE(k, z)}{\pi\sqrt{1 - k^2}}. \tag{24}$$

If l be the arc length over a quarter wave, we have

$$l = \frac{2bE}{\pi\sqrt{1 - k^2}}, \tag{25}$$

where

$$E = \int_0^{\pi/2} \sqrt{1 - k^2 \sin^2 z}\, dz$$

and is called the complete elliptic integral of the second kind. Since during the buckling increment the arclength remains unchanged,

$$\frac{dl}{dk} = 0. \tag{26}$$

From (25) and (26) we obtain:

$$\frac{2}{\pi(1 - k^2)} \left[\sqrt{1 - k^2}\left(b\frac{dE}{dk} + E\frac{db}{dk}\right) + \frac{bEk}{\sqrt{1 - k^2}}\right] = 0$$

or, when $(1 - k^2) \neq 0$,

$$\frac{(1 - k^2)}{k} b(E - K) + (1 - k^2)E\frac{db}{dk} + bEk = 0, \tag{27}$$

since according to the properties of complete elliptic integrals (Dutta & Debnath 1965, p. 187),

$$\frac{dE}{dk} = \frac{E - K}{k},$$

where K is the complete elliptic integral of the first kind (Hancock 1958). Dividing both sides of eqn. (27) by $b(1 - k^2)$ we obtain

$$\frac{E}{b}\cdot\frac{db}{dk} = \frac{K - E}{k} - \frac{Ek}{1 - k^2}$$

or,

$$\Delta k \approx \frac{E\dfrac{\Delta b}{b}}{\dfrac{K - E}{k} - \dfrac{Ek}{1 - k^2}}, \tag{28}$$

where

$$\Delta k = \frac{dk}{db}\cdot\Delta b.$$

Since α is the angle between the x_3-axis and the S-surface at the point of inflection, and $l_{(3S)3}$ is the cosine of the angle between the x_3-axis and the normal to the S-surface,

$$k = \sin\alpha = l_{(3S)3}. \tag{29}$$

Therefore, for the point of inflection of the fold, the rotation of the S-surface due to the buckling increment is

$$\Delta\alpha = \sin^{-1}(k + \Delta k) - \sin^{-1} k \tag{30}$$

where Δk and k are given by eqns. (28) and (29), respectively. The values of E and K for a particular value of k can be obtained from a table of complete elliptical integrals (Spenceley & Spenceley 1947, Belyakov *et al.* 1965) or by series expansion (Peirce 1956, p. 72). The direction cosines of the S-pole and lineation are then

$$l_{(4S)i} = c'_{ij}l_{(3S)j} \tag{31a}$$

and

$$l_{(4L)i} = c'_{ij}l_{(3L)j}, \tag{31b}$$

where, as in eqn. (10),

$$c'_{ij} = \cos(\Delta\alpha)\delta_{ij} + (1 - \cos\Delta\alpha)l_{(3F)i}l_{(3F)j} - \sin(\Delta\alpha)\varepsilon_{ijk}l_{(3F)k} \tag{31c}$$

with summation over the repeated suffix. Positive and negative values of $\Delta\alpha$ give the orientations of S and L at the two points of inflection of the fold. Note that at step 4 the orientation of the fold axis and the angle between the lineation and the fold axis remain unchanged, so that

$$l_{(4F)i} = l_{(3F)i} \tag{32a}$$

and

$$P_{(4)} = P_{(3)}. \tag{32b}$$

Structural elements at intermediate points. Let Q_1 and Q_2 be the positions of a point on the fold profile before and after the incremental buckling. Their ξ-coordinates are respectively b_1c_1 and b_2c_2. From eqns. (24) and (25) we find

$$\frac{s}{l} = \frac{E(k, (\pi/2)c)}{E}. \tag{33a}$$

Since s and l do not change during the buckling increment,

$$\frac{E(k_2, (\pi/2)c_2)}{E_2} = \frac{E(k_1, (\pi/2)c_1)}{E_1} \tag{33b}$$

where E_1 and E_2 are the complete elliptic integrals of the second kind corresponding to k_1 and k_2, respectively. Hence

$$E(k_2, (\pi/2)c_2) = E(k_1, (\pi/2)c_1)E_2/E_1. \tag{34}$$

Since all quantities on the right-hand side of eqn. (34) are known and k_2 is also known, it is theoretically possible to determine $(\pi/2)c_2$, the upper limit of the incomplete elliptic integral on the left-hand side. In practice $E(k_2, (\pi/2)c)$ was expanded into a power series (Peirce 1956, p. 72) up to the eighth power of c, and the sum of the series was repeatedly calculated by decreasing the value of c from that of c_1 by a small amount successively, till the difference from the known value of $E(k_2, (\pi/2)c_2)$ became negligibly small. The corresponding value of c was taken as c_2. After obtaining c_2, the dip angle α' at the point Q_2 was obtained from the relation

$$\tan\alpha' = \tan\alpha \cdot \cos[(\pi/2)c_2]. \tag{35}$$

The direction cosines of S are then obtained from (17a) and (17b) by replacing the subscripts $(3S)$ by $(4S)$ and $(3F)$ by $(4F)$. The direction cosines of L are given by equations similar to eqn. (3) after replacing l by l', $P_{(0)}$ by $P'_{(3)}$ and the subscripts $(0L)$ by $(4L)$ and $(0S)$ by $(4S)$. $P'_{(3)}$ is given by eqn. (18).

The structural elements at the hinge will have the same orientations as those in step 3.